COMPLETED

NASA Technical Paper 1669

ORIGINAL

Nonlinear, Three-Dimensional Finite-Element Analysis of Air-Cooled Gas Turbine Blades

Albert Kaufman and Raymond E. Gaugler

APRIL 1980

NASA

22

NASA Technical Paper 1669

Nonlinear, Three-Dimensional Finite-Element Analysis of Air-Cooled Gas Turbine Blades

Albert Kaufman and Raymond E. Gaugler
Lewis Research Center
Cleveland, Ohio

NASA
National Aeronautics
and Space Administration

**Scientific and Technical
Information Office**

1980

Summary

Cyclic stress-strain states in cooled turbine blades were computed for a simulated mission of an advanced, high-bypass-ratio, turbofan engine being studied for use in the 1990's. The assumed flight mission consisted of a 5-second takeoff transient, a 5-minute hold at maximum takeoff, a 30-minute hold at maximum climb, a 90-minute hold at cruise, and a 5-second descent transient. Airfoil-effective-stress, plastic-strain, and creep-strain distributions as functions of mission time were computed using the MARC nonlinear, finite-element computer program.

Four cases were studied: (1) an all-impingement-cooled airfoil using both a typical and a slightly flatter, gas-temperature profile and (2) two impingement-cooled turbine-blade airfoils with leading-edge holes for film cooling. Analyses were also performed for these cases using a one-dimensional beam-theory program.

The results show that creep was the predominant damage mode (ignoring oxidation and hot corrosion) and that the leading edge inside the wall was the distress location. The introduction of leading-edge film-cooling holes reduced the airfoil creep lives. An angled hole was less detrimental than a hole normal to the airfoil surface. Creep strains from the one-dimensional analyses gave reasonable agreement with the MARC analyses for the all-impingement-cooled airfoil, but not for the impingement-plus-film-cooled airfoils, even with the application of Neuber strain concentration factors. Considering the rapid solution time of the one-dimensional analysis method, it appears to be useful for all-impingement-cooled airfoils where creep is the predominant damage mode.

Introduction

Air-cooled turbine-blade airfoils in high-pressure stages of advanced aircraft engines are subject to low cycle fatigue resulting from repeated inelastic strains during engine operation. To accurately determine the airfoil cyclic lives, it is necessary to compute the transient and steady-state temperatures and the accumulated inelastic strains over the entire aircraft mission.

In recent years nonlinear finite-element programs such as MARC (refs. 1 and 2) have become available for three-dimensional analysis of structures involving cyclic creep and plasticity. Aside from their limited use as analytical research tools, these nonlinear programs have not been used in turbine design because of the extensive work and computing times involved and the need for more accurate transient thermal calculation methods. Past practice in airfoil inelastic stress analysis has been to use one-dimensional programs based on the beam theory assumption that plane sections remain plane. Although these programs are relatively easy to use, they are based on assumptions that are of questionable validity for airfoil problems involving small aspect ratios with three-dimensional stress states, and they are incapable of directly considering stress risers such as film-cooling holes.

The primary purpose of this study was to gain a greater understanding of blade damage modes, film-cooling-hole effects, and the effects of small changes in gas profile on cooled blades in advanced engines through the use of a nonlinear, three-dimensional, finite-element analysis program. A secondary purpose was to evaluate the applicability of a simpler, one-dimensional beam theory program.

The temperatures and stress-strain states in an all-impingement-cooled turbine blade airfoil and in two impingement-plus-leading-edge-film-cooled airfoils were studied. An advanced, transient, thermal-analysis program, TACT1 (ref. 3), and the MARC, nonlinear structural-analysis programs were employed. The thermostructural analyses were based on a simulated mission comprising the takeoff, climb, cruise, and descent of an advanced-technology, commercial aircraft engine. Airfoil temperatures, stresses, strains, and predicted fatigue-creep lives are compared for four cases: Case 1 represented an all-impingement-cooled turbine-blade airfoil with a typical gas-temperature profile. Case 2 represented the same configuration with a flatter gas-temperature profile. Cases 3 and 4 represented impingement-cooled turbine-blade airfoils with normal or radially angled leading-edge film-cooling holes with the typical gas-temperature profile. The effects of oxidation and hot corrosion were not considered in this study.

Analytical Procedure

The analyses were based on the operating conditions of a first-stage turbine blade in a high-bypass-ratio turbofan engine being studied for use in the 1990's.

Conditions of Analysis

The blade airfoil was 3.8 centimeters in both span and chord and had a hub-to tip radius ratio of 0.85. The assumed blade material was cast IN 100 alloy.

The assumed power settings for the mission (as shown in fig. 1) consisted of a 5-second transient from idle to maximum takeoff, a 5-minute hold at maximum takeoff, a 30-minute hold at maximum climb, a 90-minute hold at cruise, and a 5-second transient from cruise back to idle; no engine shutdown was considered in the mission. The mission cycle was divided into 34 time increments for the analysis. Two radial gas-temperature profiles (fig. 2) were condidered in this study. For profile A, which represented typical gas conditions, the effective gas temperature relative to the rotating blade (blade relative effective gas temperature) at midspan cycled between 679° C at idle and 1400° C at maximum takeoff. The flatter radial gas profile B cycled between midspan temperatures of 669° C at idle and 1378° C at maximum takeoff. The average gas temperature was identical for profiles A and B. At maximum takeoff the gas-inlet total pressure was 2858 kilopascals. The coolant-to-gas flow ratio at each operating point was essentially constant for all the cooling configurations under study (0.116 to 0.118 at maximum takeoff).

The basic airfoil impingement-cooling configurations are shown schematically in figure 3. Four cases were studied (table I): an all-impingement-cooled airfoil using both the typical (A) and flatter (B) profiles (cases 1 and 2) and two impingement-cooled airfoils with film-cooled leading edges using gas profile A. The configurations with film-cooled leading edges were approximated with a single row of 0.05-centimeter-diameter holes spaced 10 diameters apart; one configuration had the holes normal to the surface (case 3), and the other had the holes angled 30° to the surface in the spanwise direction (case 4). The gas and coolant conditions used for the analyses are specified in table I.

TABLE I. — CONDITIONS FOR THE ANALYSIS

(a) Gas temperature conditions

Case	Airfoil cooling configuration	Gas temperature profile (a)
1	All impingement	A
2	All impingement	B
3	Impingement plus leading-edge film cooling, holes normal to surface	A
4	Impingement plus leading-edge film cooling, holes 30° to surface	A

(b) Mission conditions

Simulated flight condition	Coolant- to gas-flow ratio	Coolant temperature, °C	Gas and coolant inlet pressure, kPa
Idle	0.081 - 0.088	260	689
Maximum takeoff	.116 - 0.118	538	2858
Maximum climb	.102 - 0.106	538	1303
Cruise	.098 - 0.101	538	1242

Analytical Methods

Transient and steady-state temperatures were computed with the TACT1 thermal analysis program. TACT1 was developed at Lewis to compute time-dependent, three-dimensional temperature distributions in airfoils cooled by impingement and crossflow convections. The program is also capable of handling limited film cooling; however, the effect of film-cooling-hole angle is not considered nor is the detailed temperature distribution around the hole determined. The TACT1 program capabilities are more fully described in reference 3.

Airfoil stress-strain states as a function of mission time were computed using the MARC nonlinear, finite-element, structural-analysis program. This program can perform cyclic plastic and creep-strain calculations in a series of time increments for a series of engine missions. In the analyses presented in this study, the computations were continued until the start of descent on the second mission cycle in order to eliminate from consideration the nonrecurring plastic strain induced during the initial mission. The computations for case 2 only were carried out for five mission cycles in order to study the creep relaxation.

Plastic-strain behavior was based on the incremental theory of plasticity using the von Mises yield criterion. Although a number of hardening rules were considered, including kinematic hardening, there was never sufficient stress reversal during the descent part of the mission to cause reversed plastic flow. Material creep behavior was represented by a von Mises yield criterion and a temperature-dependent exponential creep law. Centrifugal loads, gas-pressure loads as calculated from a blade-to-blade aerodynamic analysis, and local metal temperatures from TACT1 for each mission increment were input, and calculated stresses and strains output at each of 27 Gaussian integration points in each element. The centrifugal loading included the mass of the impingement insert (assumed to be uniformly distributed along the span) and a tip cap. The temperature-stress-strain results presented herein for the inner and outer surfaces of the airfoil shell represent results for Gaussian integration points at a distance approximately 11 percent of the local wall thickness from the surface under consideration.

Structural analyses were also performed using a one-dimensional, beam-theory program. The one-dimensional analyses were based on the same thermal and mechanical loading cycles and material properties as were used in the MARC analyses and included the effects of centrifugal restoring moments.

Finite-Element Analysis

The finite-element model of the all-impingement-cooled airfoil (cases 1 and 2) and impingement plus-leading-edge-film-cooled airfoil (case 3) are illustrated in figure 4. The airfoil configurations were modeled with 20-node, isoparametric, three-dimensional elements. The finite-element network for the leading-edge-film-cooled airfoil had 46 elements with 405 nodes, and the all-impingement-cooled airfoil had 39 elements with 349 nodes. The all-impingement-cooled and leading-edge-film-cooled airfoils had 977 and 1145 unsuppressed degrees of freedom, respectively. Each mission cycle required from 15 to 25 hours of accumulated Univac 1110 computer time.

The effect of the blade attachment, which was not modeled, was considered by fixing the airfoil hub in the spanwise direction. The airfoil was prevented from rigid body motion by constraining the hub leading-edge node in all directions and a hub trailing-edge node in the circumferential direction.

Because of limitations of computer storage and speed, only one leading-edge hole was modeled for cases 3 and 4. A check of the accuracy of the analysis for the leading-edge film-cooled model of figure 4 with the hole axis normal to the surface was obtained by subjecting the airfoil to a uniformly distributed, mechanical stress in the spanwise direction at a uniform temperature. An elastic stress-concentration factor of 2.85 was obtained for a station 0.003 centimeter from the hole rim; this compares with a theoretical stress-concentration factor of 3.0 at the rim of a central hole in a plate subjected to a uniaxial mechanical load.

A potentially significant error is introduced into the analysis by using only one modeling hole because the presence of adjacent holes tends to reduce the stress concentration and the local wall stiffness. This type of modeling error, as well as inadequate knowledge of cyclic material properties, preclude quantitative accuracy but should not affect the qualitative evaluation of the airfoil cooling configuration study or the qualitative comparisons of the one- and three-dimensional analyses. According to Peterson (ref.4), the theoretical stress-concentration factor for a plate with a single row of holes and a tensile load in the direction of the line of the holes is 2.9 for a spacing of 10 diameters compared with 3.0 for a single hole. To give consideration to these effects, the film-cooling hole in the finite-element model was placed at one-sixth of the span height from the airfoil hub rather than at one-third of the span, which would be a slightly more critical span location. The one-sixth position was also a some-

what more convenient location for modeling a radially angled hole. It is believed that the analysis would be relatively insensitive to small variations in the span position of the hole.

Stress-strain and monotonic creep properties were obtained for cast IN 100 alloy from reference 5; cyclic creep properties were not available for this alloy. These data were input into MARC as functions of temperature. The program then interpolates from these data for the temperature at any Gaussian integration point.

Results and Discussion

Cyclic Metal Temperatures

Computed airfoil leading-edge-stagnation-point, trailing-edge, and average temperatures at midspan are shown in figure 5 as functions of elapsed time during the mission for the four cases. Since the heat-transfer analysis did not consider the effect of the film-cooling hole angle, the thermal cycles for cases 3 and 4 were identical.

A number of features were common to the temperature transients for all the cases. The leading-edge inside wall temperature was colder than the average temperature throughout the mission; therefore, the thermal stresses were always tensile and additive to the centrifugal stresses. The outside wall temperatures at the leading and trailing edges were always hotter than the average temperature during takeoff, climb, and cruise, indicating compressive thermal stresses. At the maximum takeoff condition, where the gas pressure was highest, the temperature difference between the leading-edge inside and outside surfaces was about 150° C at midspan. The maximum metal temperatures reached during the mission were about 1050° C for all four cases and also occurred at maximum takeoff.

Comparison of cases 1 and 2 (figs. 5(a) and (b)) shows that the major thermal effect of changing from gas profile A to the flatter profile B was to reduce the leading-edge, trailing-edge, and average temperatures about 11° C at the takeoff, climb, and cruise hold-time conditions. The overall bulk temperature (not shown in the figure) did not change. Film cooling in cases 3 and 4 resulted in a leading-edge outside surface temperature that was about the average temperature at climb (fig. 5(c)). The leading-edge temperature in cases 3 and 4 (fig. 5(c)) was about 70° C cooler than in the all-impingement-cooled case 1 (fig. 5(a)).

Metal-temperature contours at cruise for the inside and outside surfaces of the airfoil pressure and suction sides are presented in figure 6 for case 1, which was used as the baseline case, in figure 7 for case 2, and in figure 8 for cases 3 and 4. In all cases a maximum metal temperature of about 1000° C was calculated for cruise at approximately midspan. This maximum temperature occurred at both the leading and trailing edges in cases 1 and 2 and at the trailing edge in cases 3 and 4. The coolest airfoil temperature was always at the leading-edge inside wall near the blade tip.

Effective Stress-Strain Distributions

Von Mises effective-stress, plastic-strain, and creep-strain contours for the end of the second mission cruise cycle are shown in figures 9 to 11 for each of the four cases at the surface where the maximum values occurred. As expected, the maximum stresses were at the inside walls where the temperatures were coldest. The highest stressed span locations were at the airfoil hub for all-impingement-cooling cases 1 and 2 (figs. 9(a) and (b)) and at the hole rim for film-cooling cases 3 and 4 (figs. 9(c) and (d)).

Results of the analyses indicated that the predominant damage mode for all cases was creep. The location of maximum effective creep strain (henceforth called the "critical location") was at the inside wall of the leading-edge region at 33-percent span height for cases 1 and 2 (figs. 10(a) and (b)) and adjacent to the hole rim for cases 3 and 4 (figs. 10(c) and (d)). The critical locations for the all-impingement-cooled configurations were slightly to the suction side of the leading edge in case 1 and slightly to the pressure side of the leading edge in case 2. The total effective strains at the critical location were either the highest or close to the highest total effective strain values in the airfoils. Case 4 was unusual in that the critical location for creep shifted from the suction side of the film-cooling hole on the first mission cycle to the pressure side of the hole on the second mission cycle.

All of the plastic strains shown in figure 11 were incurred during the takeoff transient on the initial mission cycle; no further plastic-strain changes took place during the climb and cruise parts of the mission or during the second mission cycle. The highest plastic strains occurred at the leading edge at 33 percent span on the outside surface for the all-impingement-cooling cases 1 and 2 (figs. 11(a) and (b)) because of high outside surface temperature. The maximum plastic strain for the film-cooling cases 3 and 4 (figs. 11(c) and (d)) occurred on the inside surface at the hole rim.

Effective Stress-Strain Cycles

Effective stress-temperature and strain-temperature cycles for the critical airfoil locations are presented in figures 12 and 13, respectively, for the period between the end of cruise on the first and second mission cycles. The highest stresses and total strains were reached during or near maximum takeoff. Strain ratcheting, largely due to creep effects, occurred between the beginning and end of the cycle. The stress and total strain levels, ranges, and ratcheting were considerably greater for the film-cooling cases 3 and 4 than for the all-impingement-cooling cases 1 and 2.

Effective creep strains at the critical locations are shown in figure 14 up to the end of cruise on the second mission cycle where the analyses were normally terminated. The largest creep-strain changes took place during cruise for the all-impingement-cooling cases 1 and 2 and during maximum takeoff for the film-cooling cases 3 and 4. Progressive stress relaxation under cycling caused a 35- to 45-percent reduction in the creep-strain increment for cases 1 to 3 and a 72-percent reduction for case 4 during the second mission cycle as compared with the first mission cycle. Although case 4 exhibited the highest creep-strain level, the creep increment for the second mission cycle was less than that of case 3 because of the greater creep relaxation.

The strain cycles shown in figures 13 and 14 are summarized in table II. Also presented are the maximum effective total strains reached on the first mission cycle; since there were no initial residual strains, these values were assumed to be equivalent to the total-strain ranges for a cycle where the engine is shut down at the completion of every mission.

Using case 1 as a basis of comparison, the major effect of the flatter gas-temperature profile was to decrease the creep-strain range per cycle about 20 percent. There was also an increase in total-strain range for case 2, but the total-strain levels for both all-impingement-cooling cases were too small to have any significant effect on blade life. Again using case 1 as a basis for comparison, the effect of normally oriented, leading-edge film-cooling holes (case 3) was to increase the creep-strain range by 100 percent and the total-strain range by 230 percent for the mission analyzed and 150 percent for an engine shut down after each mission. Angling the holes 30° radially to the surface (case 4) resulted in smaller total- and creep-strain increments per cycle than having the holes normal to the surface (case 3). The increases in strain ranges in case 4 compared with case 1 were 39 percent in creep strain, 220 percent in total strain for the mission, and 120 percent in total strain for an engine shut down after each mission.

Comparison of One- and Three-Dimensional Analyses

One-dimensional beam-theory analyses were also performed for cases 1 and 2 for the 33-percent airfoil span section. The analyses were based on the same thermal and mechanical loading cycle and material properties as were used in the MARC analyses and included the effects of centrifugal restoring moments. The analytical method is based on the beam theory assumption that plane sections remain plane; the method is discussed in greater detail in reference 6. The maximum total- and creep-strain changes per cycle from the two analytical methods are compared in table II.

TABLE II — RESULTS OF MISSION STRAIN ANALYSIS

Case	Analysis	Maximum effective total strain range cm/cm		Maximum effective creep strain increment during second mission cycle cm/cm	Predicted nondimensional cyclic lives[b,c]
		Idle to maximum takeoff	First mission cycle[a]		
1	MARC Beam theory	0.00141 .00277	0.00234 .00281	0.000484 .000427	1.00
2	MARC Beam theory	0.00277 .00290	0.00248 .00282	0.000399 .000351	1.21
3	MARC Beam theory	0.00468 .01018	0.00602 .01368	0.000970 .000591	0.50
4	MARC Beam theory	0.00453 .01018	0.00523 .01368	0.000671 .000591	0.72

[a]Estimated values between maximum takeoff and shutdown.

[b]Based on maximum effective creep strain during second mission cycle.

[c]Life is the reciprocal of the ratio of creep strain increment for case 1 to that for the case under consideration.

The critical airfoil location from the one-dimensional analysis was on the suction side of the leading edge (location B in fig. 15), whereas the critical locations from the MARC analyses were nearer to the stagnation line (location A for case 1) and on the pressure side near the leading edge (location C for case 2). Computed creep-strain increments per mission cycle up to the 50th cycle are shown in figure 15 at locations A and B for case 1 and locations B and C for case 2. Comparison of these results with the computed creep-strain increments from the MARC analyses indicates reasonable agreement for mission cycles considered, with the one-dimensional analysis predicting somewhat higher creep strains. However, the one-dimensional solutions exaggerate the amount of creep relaxation, with the result that they predict lower creep-strain increments after the first mission cycle. The faster creep relaxation shown by the one-dimensional analysis is probably caused by forcing the displacements to lie on a plane. The results also suggest that the analyses should be carried out to at least a third mission cycle in order to attain a reasonably stable stress- and creep-strain state. The calculated maximum total strains and strain ranges from the beam-theory analyses were 14 to 20 percent higher and 79 to 96 percent higher, respectively, than those from the MARC results. The greater variation in terms of total strain range was primarily due to predicting greater residual strains on unloading with the beam-theory analysis.

Considering the relative simplicity and rapid solution time of the one-dimensional program, these results indicate that it can be used with the all-impingement-cooled airfoil shells when creep is the major damage mechanism. However, this method cannot take into account directly the stress concentration due to the presence of a film-cooling hole. An indirect approach was to multiply the nominal strains in the vicinity of the hole by a strain concentration factor of 4.24, calculated by the Neuber method (ref. 7) for a theoretical elastic-stress concentration factor of 3.0. The creep-strain increments at the hole for cases 3 and 4 (fig. 15(c)), computed using this procedure, were 50 percent less for the first mission cycle than those using the MARC analysis. The total strains and strain ranges from the beam-theory analysis were more than twice those from the three-dimensional analysis for cases 3 and 4 (table II). These results are in agreement with the conclusion of reference 7 that use of the Neuber method for biaxial stress states leads to excessively high strains and to considerable error. Further work is required to develop an adequate procedure for accounting for film-cooling-hole effects in beam-theory analyses.

Life Analyses

Strain cycling fatigue data for IN 100 at 927° C presented in reference 8 indicated the following: (1) The fatigue life from repeated cycling over the total strain ranges shown in table II would be virtually infinite for cases 1 and 2, and (2) the fatigue lives for cases 3 and 4 would be at least an order of magnitude greater than the predicted creep lives as determined from a ductility exhaustion approach (ref. 9) using the creep-strain increment during the second mission cycle. Therefore, the low-cycle fatigue lives of the airfoil configurations considered herein would be dominated by creep under the assumed engine operating conditions.

Because the creep increments per mission cycle would be reduced on subsequent cycles because of further stress relaxation, the life predictions on crack initiation are presented in table II on a nondimensionalized basis with respect to case 1. The predicted life for any case is simply the reciprocal of the ratio of the creep-strain increment for case 1 to the creep-strain increment for the case under consideration; this follows from the assumption of ductility exhaustion. The effect of using a flatter gas-temperature profile in case 2 was to increase the cyclic creep life of the all-impingement-cooled airfoil about 21 percent. The introduction of leading-edge film-cooling holes with the holes oriented normal to the airfoil surface (case 3) resulted in a 50 percent reduction in cyclic creep life; however, these results do not take into account the reduced susceptibility to oxidation and hot-corrosion damage due to the reduced leading-edge temperatures. Angling the film-cooling holes 30° radially to the surface (case 4) resulted in a 28-percent reduction in cyclic life compared with the base, all-impingement-cooled configuration (case 1).

Summary of Results

The major results of the nonlinear, three-dimensional, finite-element analyses of impingement-cooled gas-turbine-blade airfoils with and without leading-edge film cooling were as follows:

1. Creep was the predominant damage mode (neglecting oxidation and hot corrosion), and the leading-edge inside wall was the predicted distress location for all of the airfoil configurations analyzed. Plastic strains were incurred only during the takeoff transient on the initial mission cycle. Predicted fatigue lives based on the maximum total strain ranges were at least an order of magnitude greater than the predicted creep lives as determined from a ductility exhaustion approach.

2. The use of a flatter gas-temperature profile, which reduced the maximum gas temperatures at

the rotor inlet by 22° C, resulted in a 21-percent improvement in predicted creep life for the all-impingement-cooled airfoils.

3. The introduction of leading-edge film-cooling holes was detrimental to the creep lives, although it lowered the leading-edge temperatures which would tend to reduce the susceptibility to oxidation and hot-corrosion damage. For the same metal temperatures a hole with the axis angled radially was less detrimental than a hole with the axis normal to the airfoil surface.

4. One-dimensional analyses gave reasonable agreement with the three-dimensional analyses for the all-impingement-cooled configuration (cases 1 and 2); however, they did not give similarly good agreement when used in conjunction with a Neuber strain-concentration factor for the film-cooled configuration. Considering the rapid solution time, the one-dimensional analysis appears to be useful for all-impingement-cooled airfoils where creep is the predominant damage mode.

Lewis Research Center,
National Aeronautics and Space Administration,
Cleveland, Ohio, July 26, 1979,
505–02.

References

1. MARC General Purpose Finite Element Analysis Program. Vols. A and B. Users Manual. Marc Analysis Research Corp., 1979.
2. MARC Program Input. Vols. C, D, E. Users Manual. Marc Analysis Research Corp., 1979.
3. Gaugler, R.E.: TACT1, A Computer Program for the Transient Thermal Analysis of a Cooled Turbine Blade or Vane Equipped with a Coolant Insert. I — User's Manual. NASA TP-1271, 1978.
4. Peterson, R.E.: Stress Concentration Factors. John Wiley and Sons, Inc., 1974.
5. Fritz, L.J., and Koster, W.P.: Tensile and Creep Rupture Properties of (16) Uncoated and (2) Coated Engineering Alloys at Elevated Temperatures. (REPT-931-21300, Metcut Research Assoc., Inc.; NASA Contract NAS3-18911.) NASA CR-135138, 1977.
6. Kaufman, A.: Steady-State Stress Relaxation Analysis of Turbine Blade Cooling Designs. NASA TN D-5282, 1969.
7. Mowbray, D.F., and McConnelee, J.E.: Applications of Finite Element Stress Analysis and Stress-Strain Properties in Determining Notch Fatigue Specimen Deformation and Life. Cyclic Stress-Strain Behavior — Analysis, Experimentation, and Fatigue Prediction. Am. Soc. Test. Mater. Spec. Tech. Publ. 519, 1973, pp. 151-169.
8. Stewart, O.L., and Vogel, W.H.: Methods for Predicting Thermal Stress Cracking in Turbine Stator or Rotor Blades. (PWA-3142, Pratt & Whitney Aircraft; NASA Contract NAS3-7909.) NASA CR-54636, 1967.
9. Spera, D.A.: Comparison of Experimental and Theoretical Thermal Fatigue Lives for Five Nickel-Base Alloys. Fatigue at Elevated Temperatures. Am. Soc. Test. Mater. Spec. Tech. Publ. 520, 1973, pp. 648-656.

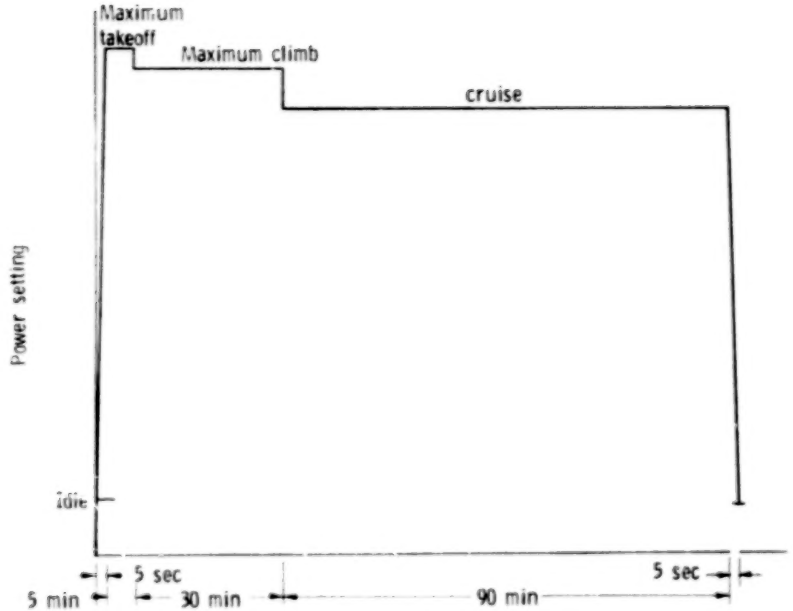

Figure 1. - Assumed power settings for mission. (Note: Abscissa time markings are not to scale.)

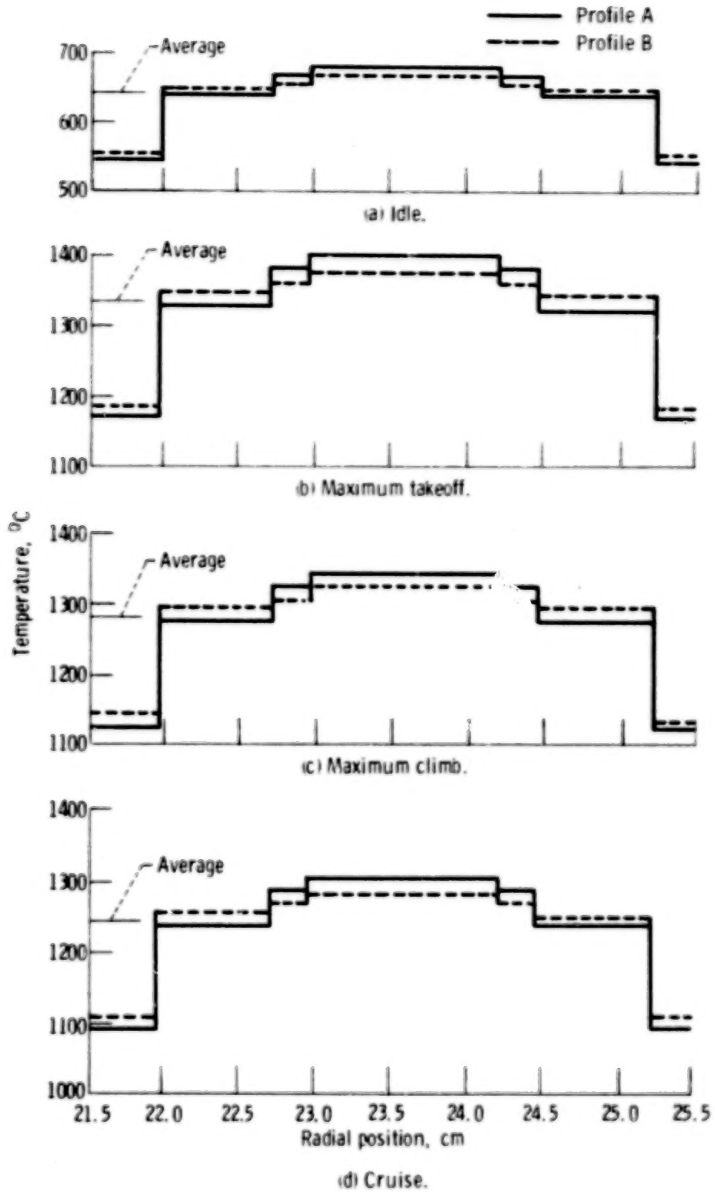

Figure 2. - Turbine blade relative effective gas temperature profiles.

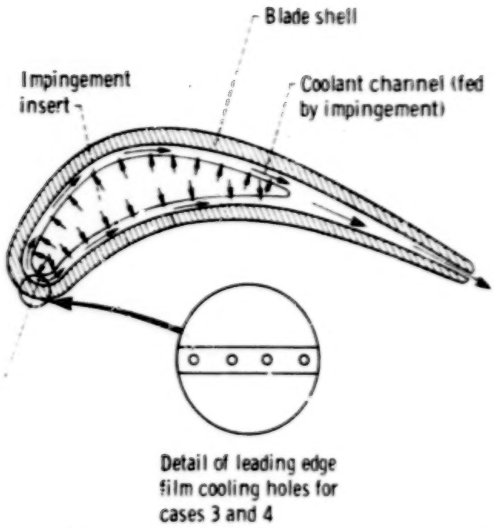
Blade shell
Impingement insert
Coolant channel (fed by impingement)
Detail of leading edge film cooling holes for cases 3 and 4

Figure 3. - Basic airfoil impingement-cooling configurations.

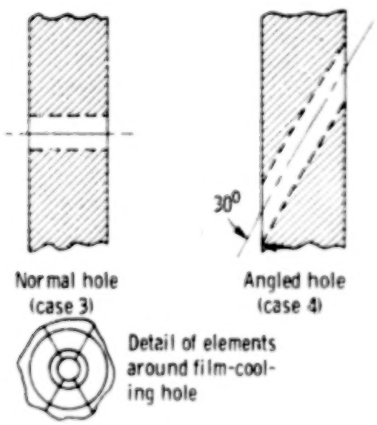

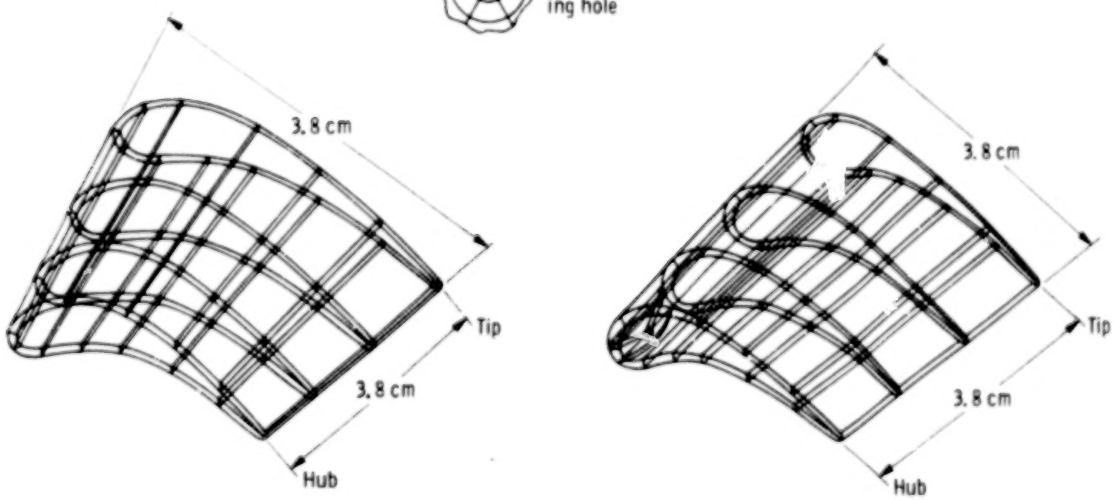

(a) All-impingement-cooled airfoil. (b) Leading-edge-plus-film-cooled airfoil

Figure 4. - Airfoil finite element models.

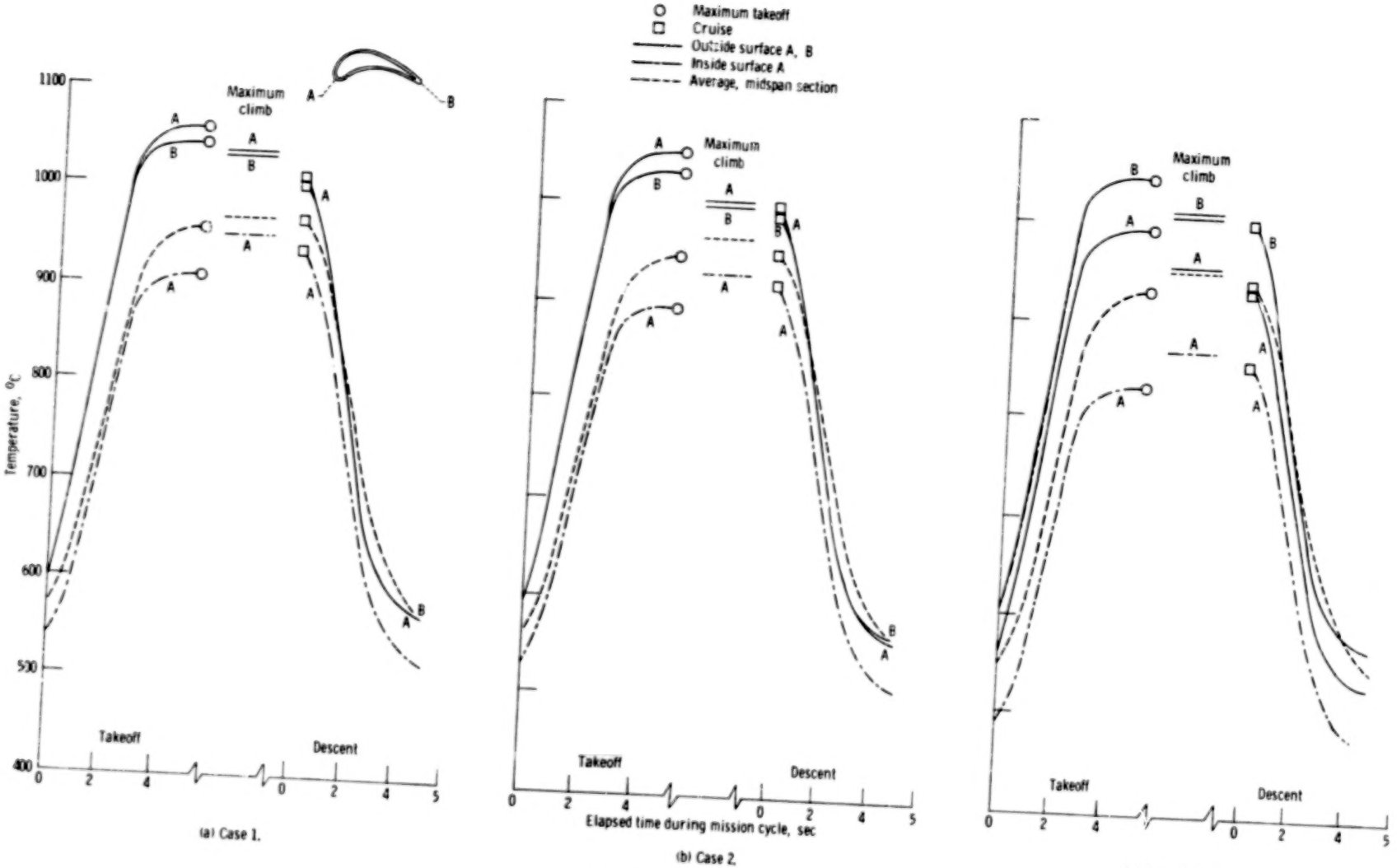

(a) Case 1.

(b) Case 2.

(c) Cases 3 and 4.

Figure 5. - Airfoil metal temperature cycle at midspan.

	(a)	(b)	(c)	(d)
1	832	827	793	777
2	849	843	816	799
3	866	866	838	821
4	887	882	854	838
5	904	904	877	860
6	927	921	893	882
7	943	943	916	899
8	966	966	938	921
9	982	982	954	943
10	999	1004	977	966

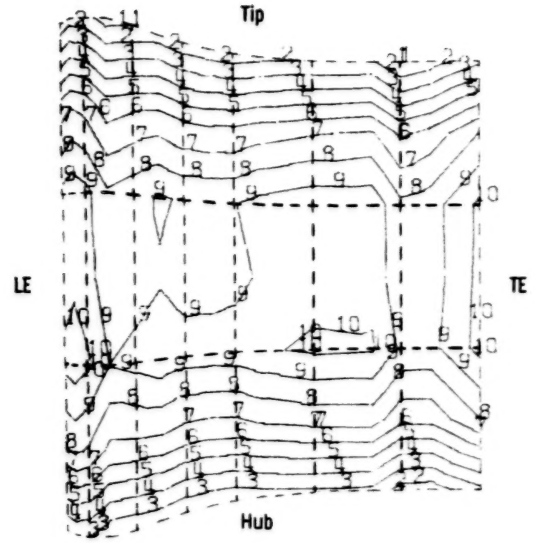

(a) Outside surface, pressure side.

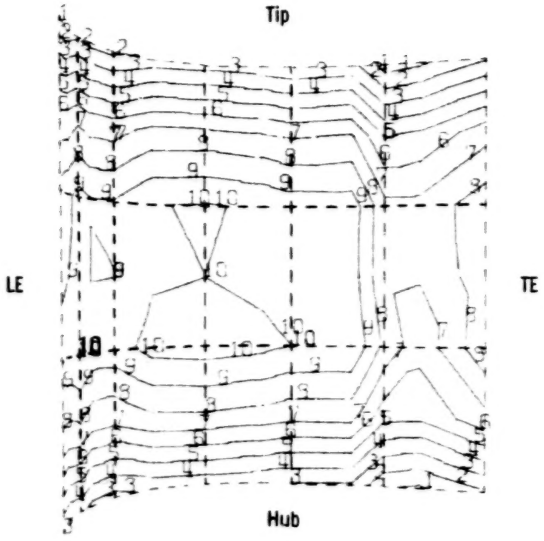

(b) Outside surface, suction side.

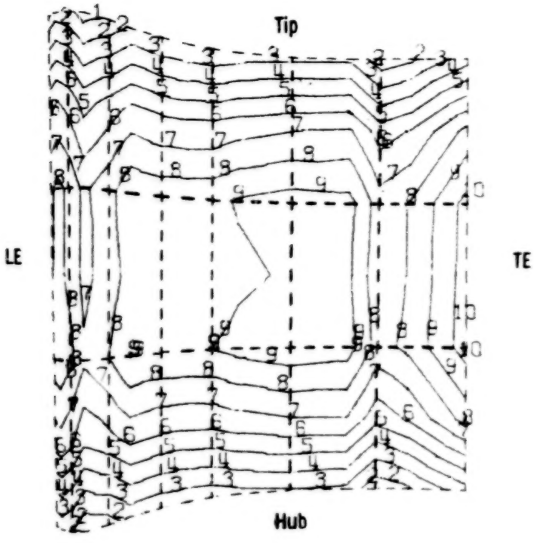

(c) Inside surface, pressure side.

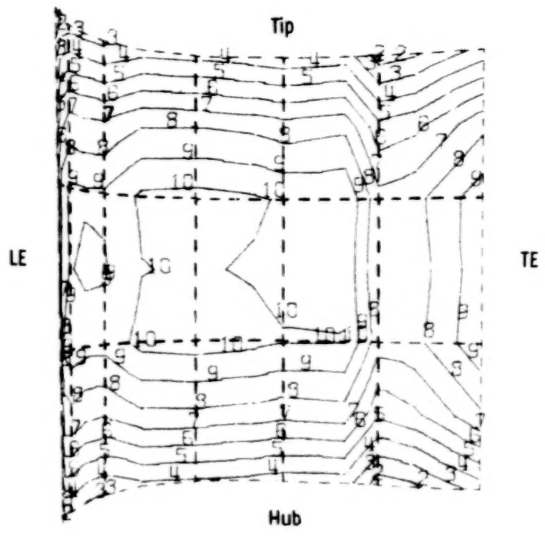

(d) Inside surface, suction side.

Figure 6. - Airfoil metal temperature distribution at cruise for case 1. LE denotes leading edge; TE, trailing edge.

	Temperature, °C			
	(a)	(b)	(c)	(d)
1	838	832	799	782
2	854	849	821	804
3	871	866	838	821
4	888	882	854	838
5	904	904	877	860
6	921	921	893	877
7	938	938	910	893
8	954	954	927	916
9	971	971	949	932
10	988	993	966	949

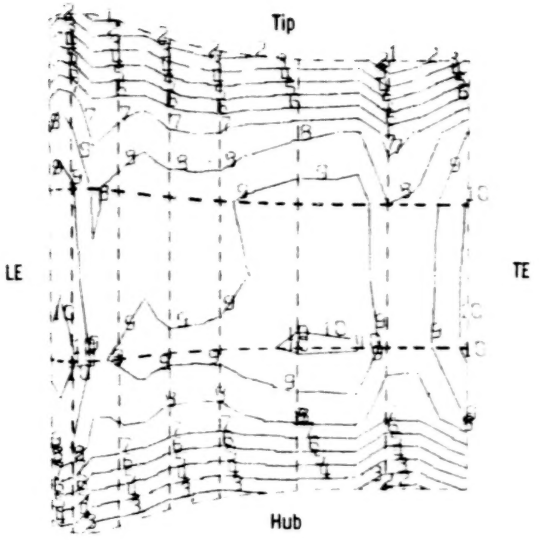

(a) Outside surface, pressure side.

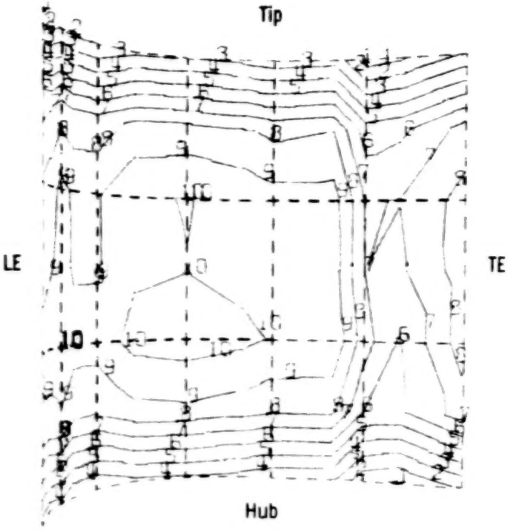

(b) Outside surface, suction side.

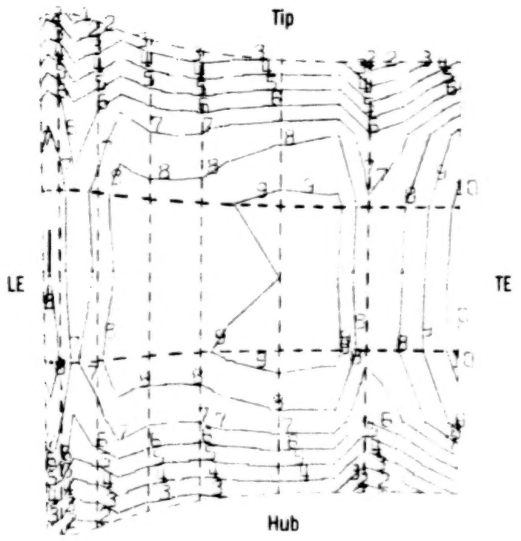

(c) Inside surface, pressure side.

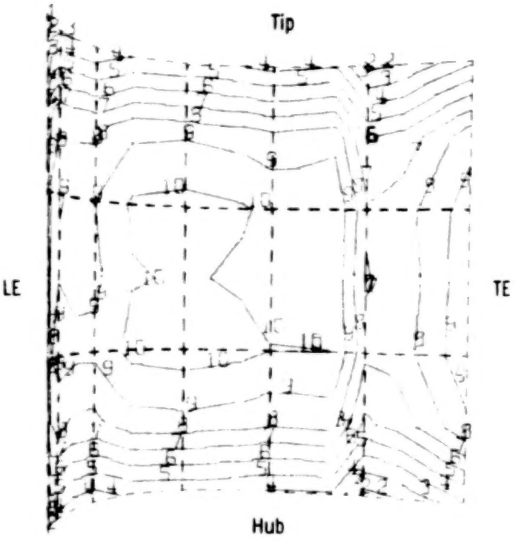

(d) Inside surface, suction side.

Figure 7. - Airfoil metal temperature distribution at cruise for case 2. LE denotes leading edge; TE, trailing edge.

	Temperature, ^{0}C			
	(a)	(b)	(c)	(d)
1	721	721	716	688
2	749	749	743	716
3	782	777	771	743
4	810	804	799	771
5	843	832	827	799
6	871	860	860	827
7	899	888	888	854
8	932	916	916	882
9	960	943	943	910
10	993	971	971	938

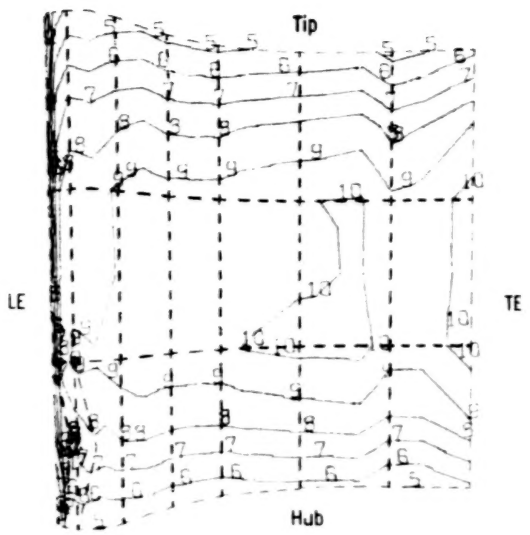

(a) Outside surface, pressure side.

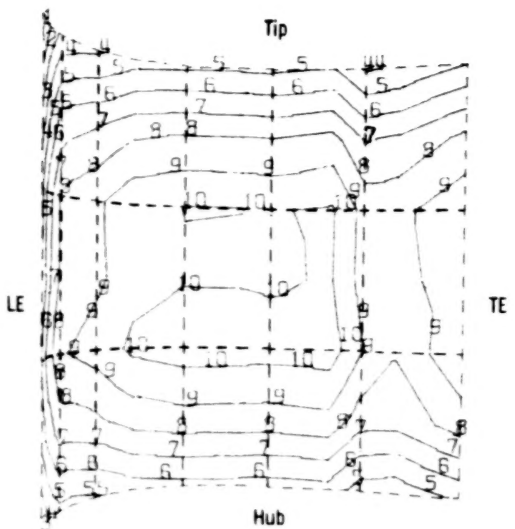

(b) Outside surface, suction side.

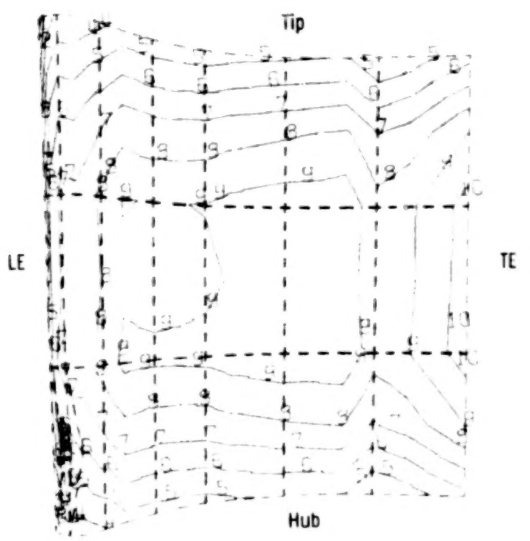

(c) Inside surface, pressure side.

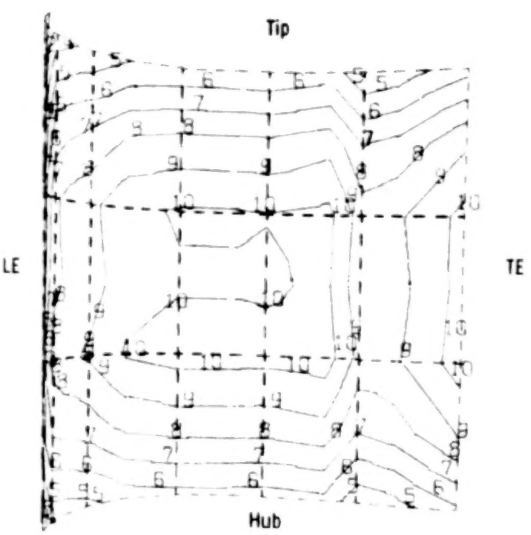

(d) Inside surface, suction side.

Figure 8. - Airfoil metal temperature distribution at cruise for cases 3 and 4. LE denotes leading edge; TE, trailing edge.

	Stress, MPa, for case -			
	1	2	3	4
1	67	49	83	83
2	98	86	120	121
3	130	123	157	159
4	161	159	192	196
5	192	195	229	233
6	223	232	265	271
7	255	269	302	308
8	286	305	339	325
9	318	343	375	383
10	349	379	411	421

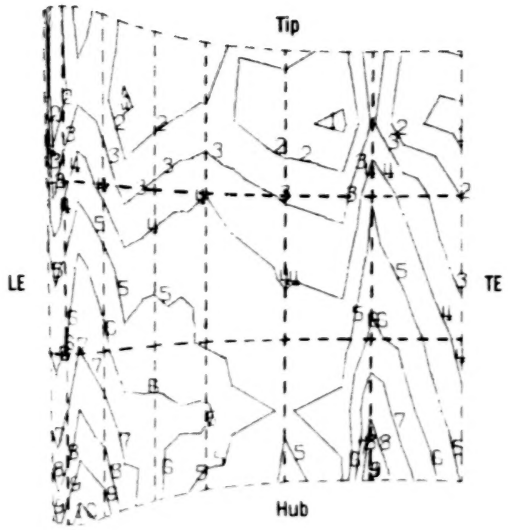

(a) Case 1, inside surface, pressure side.

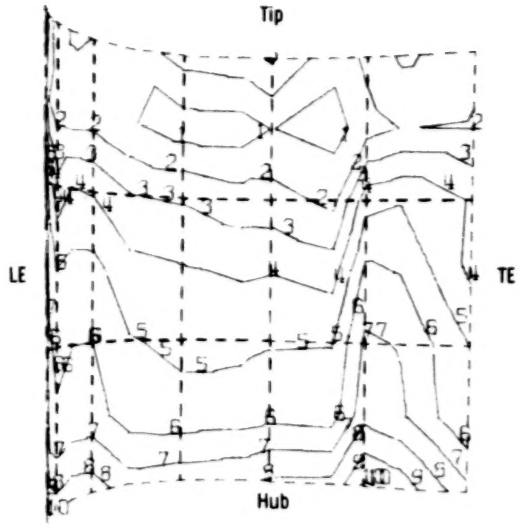

(b) Case 2, inside surface, suction side.

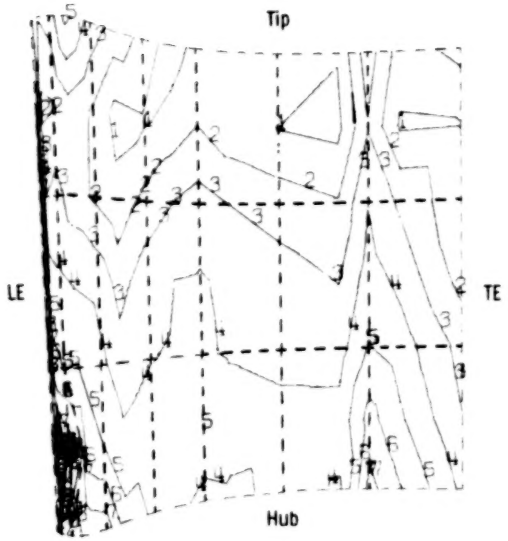

(c) Case 3, inside surface, pressure side.

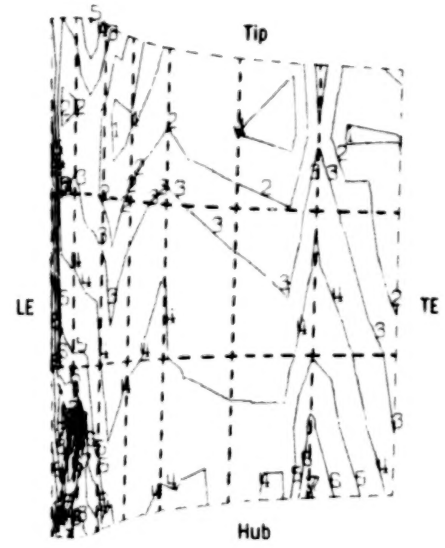

(d) Case 4, inside surface, suction side.

Figure 9. - Effective stress distributions at end of cruise (second mission cycle). LE denotes leading edge; TE, trailing edge.

Contour	Microstrain for case -			
	1	2	3	4
1	-29	29	7	73
2	116	136	19	322
3	262	244	38	571
4	408	351	57	821
5	553	459	76	1070
6	699	567	94	1320
7	845	675	1130	1570
8	990	782	1320	1820
9	1140	890	1500	2070
10	1280	998	1690	2320

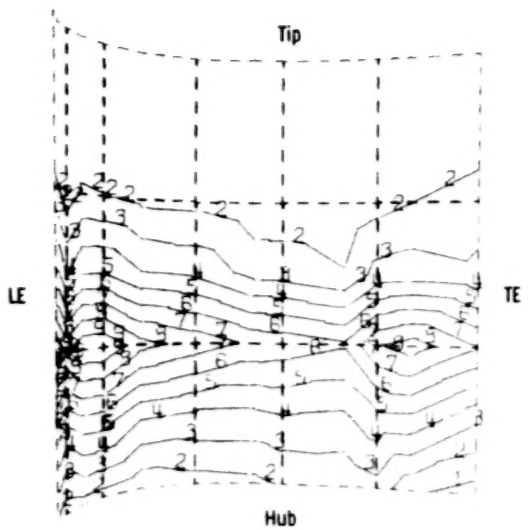

(a) Case 1, inside surface, suction side.

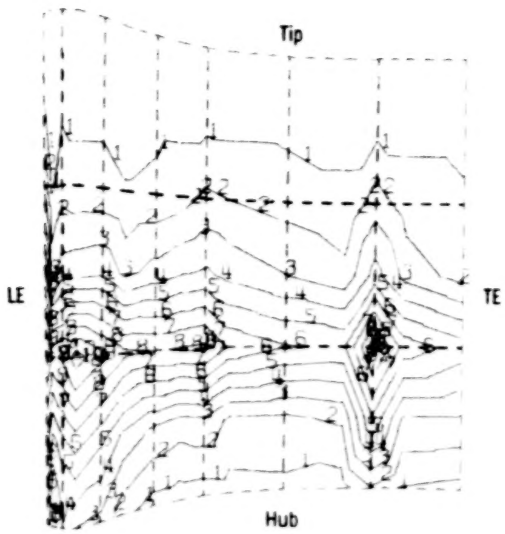

(b) Case 2, inside surface, pressure side.

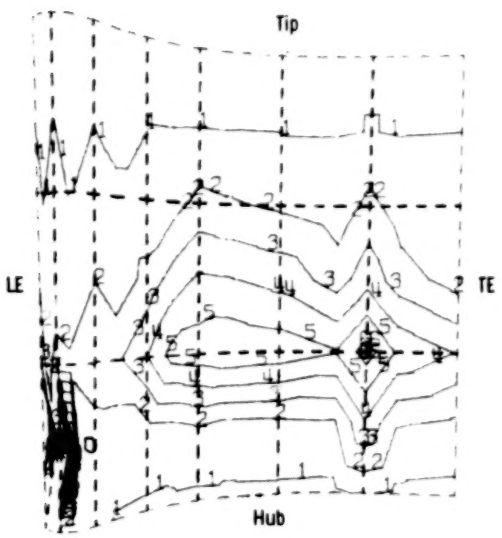

(c) Case 3, inside surface, pressure side.

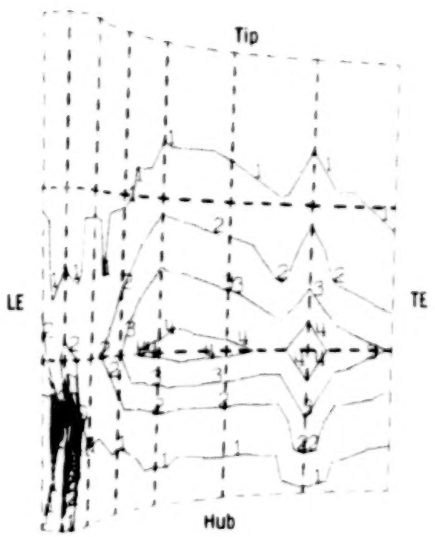

(d) Case 4, inside surface, pressure side.

Figure 10. - Effective creep-strain distributions at end of cruise (second mission cycle). LE denotes leading edge; TE, trailing edge.

Contour	Microstrain, for case -			
	1	2	3	4
1	-6	-6	38	8
2	11	9	121	130
3	27	24	204	253
4	44	38	287	375
5	60	53	370	498
6	77	68	453	620
7	93	83	536	742
8	110	97	619	865
9	126	112	702	987
10	143	127	785	1110

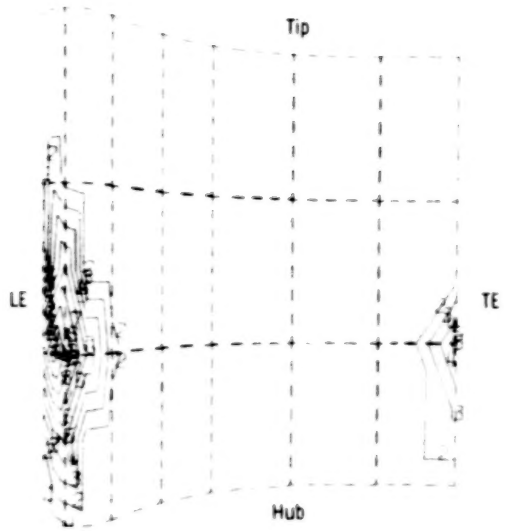

(a) Case 1, outside surface, pressure side.

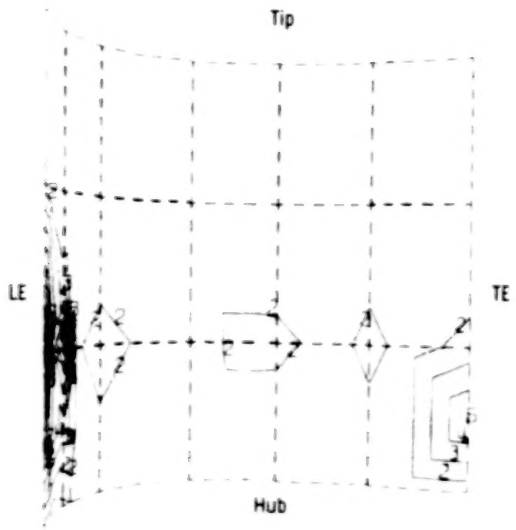

(b) Case 2, outside surface, suction side.

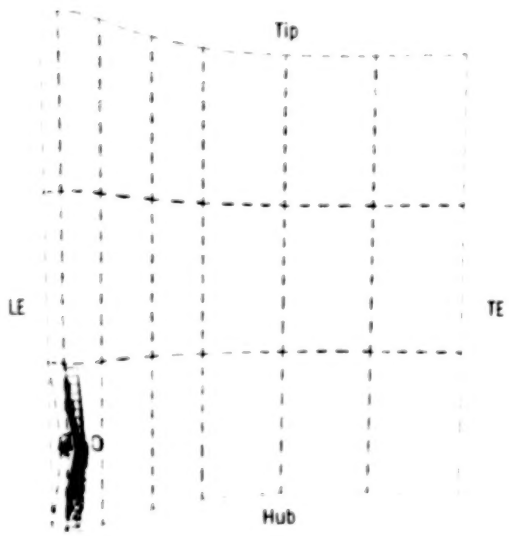

(c) Case 3, inside surface, pressure side.

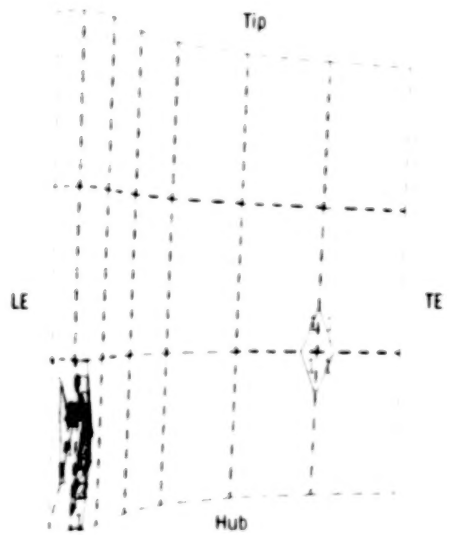

(d) Case 4, inside surface, pressure side.

Figure 11. - Effective plastic strain distributions at end of cruise (second mission cycle). LE denotes leading edge; TE, trailing edge.

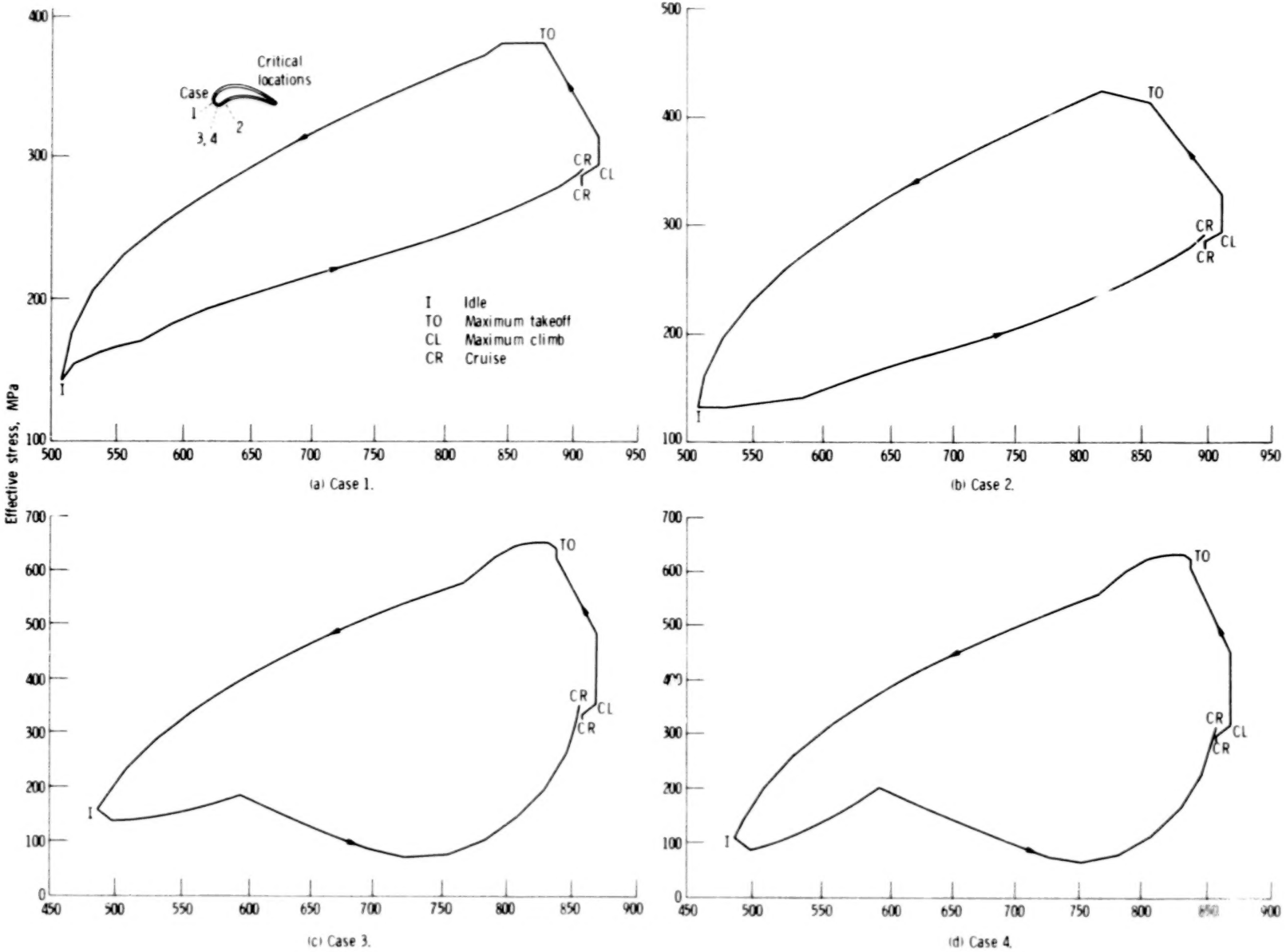

Figure 12. - Effective stress-temperature cycles for airfoil critical locations.

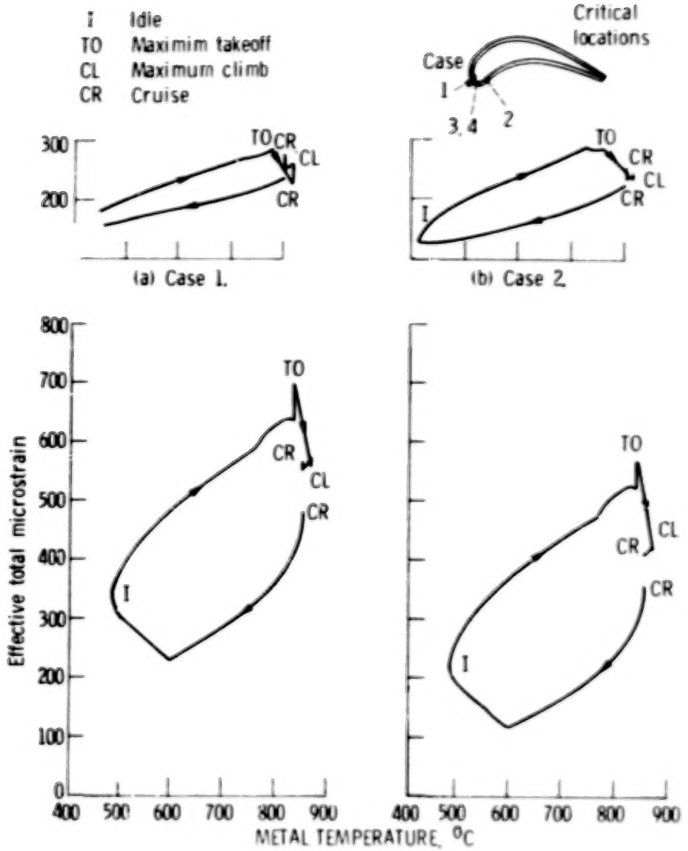

Figure 13. - Effective total strain-temperature cycles for critical airfoil locations.

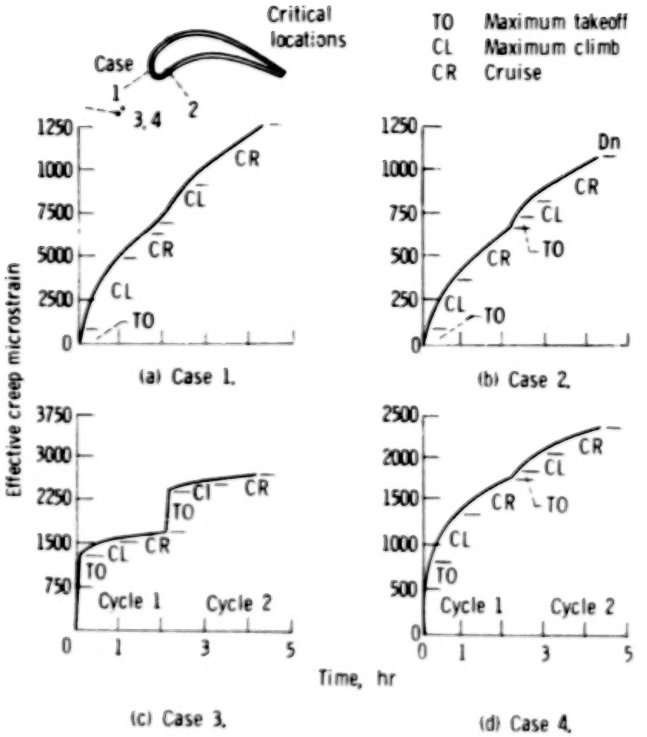

Figure 14. - Effective creep strain as function of time for critical airfoil locations.

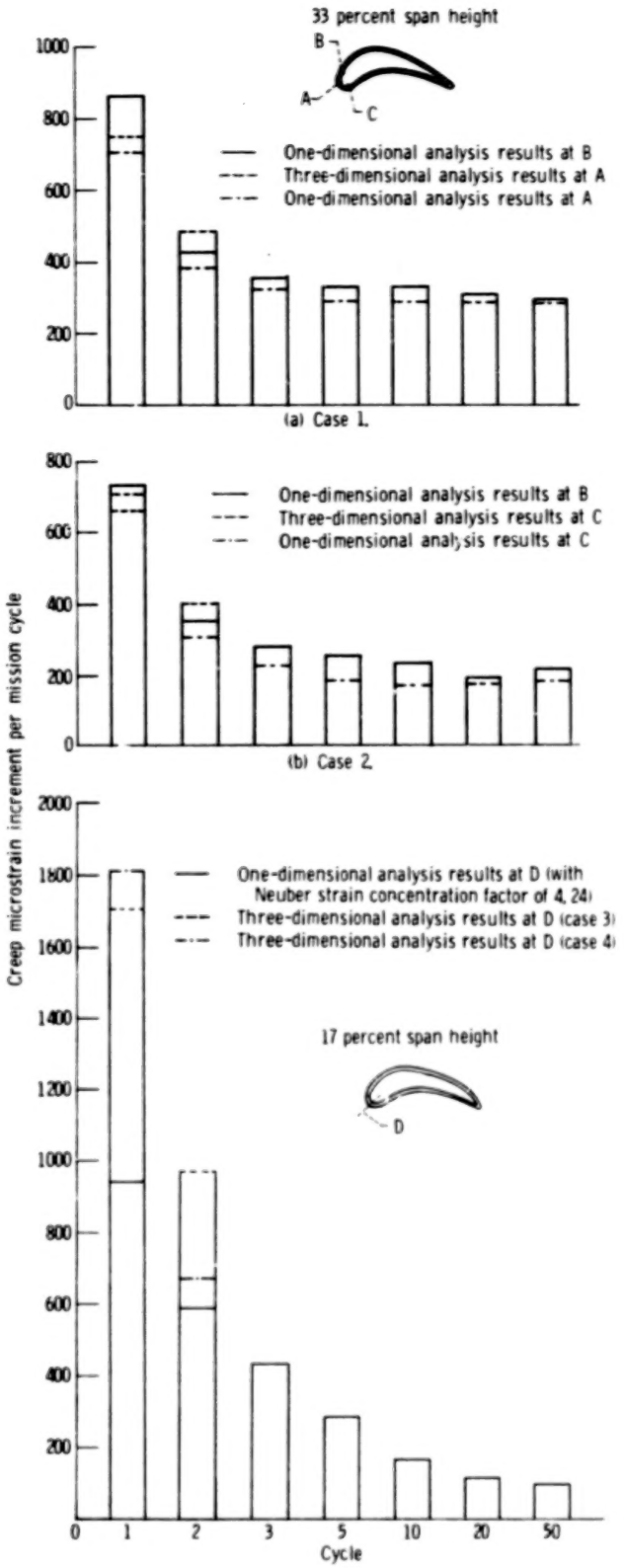
33 percent span height
B
A
C
One-dimensional analysis results at B
Three-dimensional analysis results at A
One-dimensional analysis results at A
(a) Case 1.
One-dimensional analysis results at B
Three-dimensional analysis results at C
One-dimensional analysis results at C
(b) Case 2.
Creep microstrain increment per mission cycle
One-dimensional analysis results at D (with Neuber strain concentration factor of 4.24)
Three-dimensional analysis results at D (case 3)
Three-dimensional analysis results at D (case 4)
17 percent span height
D
Cycle
(c) Cases 3 and 4.

Figure 15. - Comparison of creep-strain computations from one- and three- dimensional structural analyses.

1 Report No. NASA TP-1669	2 Government Accession No.	3 Recipient's Catalog No.
4 Title and Subtitle **NONLINEAR, THREE-DIMENSIONAL FINITE-ELEMENT ANALYSIS OF AIR-COOLED GAS TURBINE BLADES**		5 Report Date April 1980 6 Performing Organization Code
7 Author(s) **Albert Kaufman and Raymond E. Gaugler**		8 Performing Organization Report No. **E-074**
9 Performing Organization Name and Address **National Aeronautics and Space Administration** **Lewis Research Center** **Cleveland, Ohio 44135**		10 Work Unit No. **505-02** 11 Contract or Grant No.
12 Sponsoring Agency Name and Address **National Aeronautics and Space Administration** **Washington, D.C. 20546**		13 Type of Report and Period Covered **Technical Paper** 14 Sponsoring Agency Code
15 Supplementary Notes		

16 Abstract

Cyclic stress-strain states in cooled turbine blades were calculated for a simulated mission of an advanced-technology commercial aircraft engine. The MARC, nonlinear, finite-element computer program was used for the analysis of impingement-cooled airfoils, with and without leading-edge film cooling. Creep was the predominant damage mode (ignoring hot corrosion), particularly around film-cooling holes. Radially angled holes exhibited less creep than holes with axes normal to the surface. Beam-theory analyses of all-impingement-cooled airfoils gave fair agreement with MARC results for initial creep.

17 Key Words (Suggested by Author(s))	18 Distribution Statement
Analysis (Mathematics) Finite element method Turbine blades Cooling	Unclassified - unlimited STAR Category 39

19 Security Classif. (of this report)	20 Security Classif. (of this page)	21 No. of Pages	22 Price*
Unclassified	Unclassified	20	A02

* For sale by the National Technical Information Service, Springfield, Virginia 22161

NASA-Langley, 1980